Published in final edited form as:
Bone. 2014 October ; 67: 95–103. doi:10.1016/j.bone.2014.07.007.

Inkjet-based biopatterning of SDF-1β augments BMP-2-induced repair of critical size calvarial bone defects in mice

Samuel Herberg, Ph.D.[a], **Galina Kondrikova, B.S.**[a], **Sudharsan Periyasamy-Thandavan, Ph.D.**[a], **R. Nicole Howie, M.S.**[b], **Mohammed E. Elsalanty, M.D., Ph.D.**[b,e], **Lee Weiss, Ph.D.**[f,h], **Phil Campbell, Ph.D.**[g,h], **William D. Hill, Ph.D.**[a,c,e,i], and **James J. Cray, Ph.D.**[*,a,b,c,d,e]

[a]Department of Cellular Biology and Anatomy, Georgia Regents University, 1459 Laney Walker Blvd., Augusta, GA, USA

[b]Department of Oral Biology, Georgia Regents University, 1459 Laney Walker Blvd., Augusta, GA, USA

[c]Department of Orthopaedic Surgery, Georgia Regents University, 1120 15th St., Augusta, GA, USA

[d]Department of Orthodontics and Surgery, Division of Plastic Surgery, Georgia Regents University, 1120 15th St., Augusta, GA, USA

[e]Institute for Regenerative and Reparative Medicine, Georgia Regents University, 1459 Laney Walker Blvd., Augusta, GA, USA

[f]The Robotics Institute, Carnegie Mellon University, 5000 Forbes Ave., Pittsburgh, PA, USA

[g]The Institute for Complex Engineered Systems, Carnegie Mellon University, 5000 Forbes Ave., Pittsburgh, PA, USA

[h]McGowan Institute for Regenerative Medicine, 450 Technology Drive, Pittsburgh, PA, USA

[i]Charlie Norwood VA Medical Center, Augusta, GA, USA

Abstract

Background—A major problem in craniofacial surgery is non-healing bone defects. Autologous reconstruction remains the standard of care for these cases. Bone morphogenetic protein-2 (BMP-2) therapy has proven its clinical utility, although non-targeted adverse events occur due to the high milligram-level doses used. Ongoing efforts explore the use of different growth factors, cytokines, or chemokines, as well as co-therapy to augment healing.

[*]**Address for correspondence and reprints:** James J. Cray Jr., Ph. D., Medical University of South Carolina, Department of Oral Health Sciences, BSB 230G, 173 Ashley Ave, Charleston, SC 29425, crayj@musc.edu, Phone: +1-843-792-2327.

Disclosure Statement
The authors have no conflict of interest.

Methods—Here we utilize inkjet-based biopatterning to load acellular DermaMatrix delivery matrices with nanogram-level doses of BMP-2, stromal cell-derived factor-1β (SDF-1β), transforming growth factor-β1 (TGF-β1), or co-therapies thereof. We tested the hypothesis that bioprinted SDF-1β co-delivery enhances BMP-2 and TGF-β1-driven osteogenesis both *in-vitro* and *in-vivo* using a mouse calvarial critical size defect (CSD) model.

Results—Our data showed that BMP-2 bioprinted in low-doses induced significant new bone formation by four weeks post-operation. TGF-β1 was less effective compared to BMP-2, and SDF-1β therapy did not enhance osteogenesis above control levels. However, co-delivery of BMP-2 + SDF-1β was shown to augment BMP-2-induced bone formation compared to BMP-2 alone. In contrast, co-delivery of TGF-β1 + SDF-1β decreased bone healing compared to TGF-β1 alone. This was further confirmed *in vitro* by osteogenic differentiation studies using MC3T3-E1 pre-osteoblasts.

Conclusions—Our data indicates that sustained release delivery of a low-dose growth factor therapy using biopatterning technology can aid in healing CSD injuries. SDF-1β augments the ability for BMP-2 to drive healing, a result confirmed *in vivo* and *in vitro*; however, because SDF-1β is detrimental to TGF-β1-driven osteogenesis, its' effect on osteogenesis is not universal.

Keywords

Bone; Healing; Biopatterning; BMP-2; SDF-1β; TGF-β1

Introduction

Craniofacial wounds resulting from injury trauma or iatrogenic sources (e.g., tumor removal) present a major problem for surgery. Although bone has an innate capacity to heal, large defects in the calvarium are known to present with inadequate bony healing [1-3]. Autologous reconstruction has been the standard of care in these cases. However, problems exist with this approach [4], including the shortage of the amount of available bony tissue that can be harvested from the patient (i.e., ribs or iliac crest) and associated significant morbidities [5]. Allogeneic grafts or synthetic materials (e.g., cadaveric bone, hydroxyapatite, etc.) are often used as alternatives despite their limitations, often causing suboptimal outcomes [1]. More recently attention has been paid to growth factor therapies, specifically bone morphogenetic protein-2 (BMP-2), a member of the transforming growth factor-beta (TGF-β) superfamily. BMP-2 (INFUSE, Medtronic, Minneapolis, Minnesota) is FDA-approved for procedures such as sinus augmentation and spinal fusion. BMP-2 has also proved successful in other clinical applications including the treatment of acute, primary calvarial wounds [3, 4, 6-12]. However, despite its clinical utility, undo complications have been reported [13, 14]. These problems have mostly been associated with the supraphysiological BMP-2 doses utilized clinically to overcome delivery issues [15, 16]. BMP-2 therapies are also extremely expensive, in large part due to the large milligram doses currently used.

There is ongoing research to address the limitations of BMP-2 for healing bony wounds safely and effectively. One approach is the utilization of different growth factors, cytokines, or chemokines, as well as co-therapy strategies including BMP-2 to augment healing.

Stromal cell-derived factor-1 (SDF-1/CXCL12) is a member of the CXC chemokine family [17]. SDF-1 and its cognate receptor (CXCR4) are expressed constitutively in various tissues [18-20]. Among other chemokine pathways, binding of SDF-1 to CXCR4 initiates the recruitment of regenerative cells to injury sites during the acute phase of bone repair [21-23]. Furthermore, a direct regulatory role for SDF-1 signaling in BMP-2-induced osteogenic differentiation of mesenchymal cells has been reported *in vitro* [24-26] and *in vivo* [27-31] employing ectopic and orthotopic bone formation models. Transforming growth factor-beta (TGF-β) isoforms have also received some attention. TGF-β1 is a cytokine responsible for the control of cell proliferation of many cell types, including osteoblasts; thus TGF-β1 has osteogenic properties [32, 33]. TGF-β1 is expressed constitutively in healing bone fractures and plays a positive role in bone formation by the stimulation of Runx2, an early marker of osteoblastogenesis [34-39]. It may however inhibit late stage osteoblast differentiation [40]. Interestingly, TGF-β1 has cell homing properties [32] and has been shown to enhance the ability of SDF-1 in this process [41, 42].

In this study we investigated the combination of several approaches to augment bone wound healing, including highly-localized co-delivery of multiple growth factors in low-doses. We used established inkjet-based biopatterning technology [43-47] to controllably load nano-gram level doses of BMP-2, SDF-1β, and TGF-β1, or combinations thereof, into acellular DermaMatrix delivery scaffolds, which have native binding affinities for these growth factors. SDF-1β was chosen over the more abundant splice variant SDF-1α due to its greater resistance to proteolytic cleavage conferred by its additional 4 C-terminal amino acids relative to SDF-1α [1, 48, 49]. We tested the hypothesis that SDF-1β co-delivery enhances BMP-2- and TGF-β1-driven osteogenesis both *in vitro* and *in vivo* using a mouse calvarial critical size defect (CSD) model.

Materials and Methods

Animals

C57BL/6J male mice were purchased from Jackson Laboratories (Bar Harbor, ME, USA). Animals were maintained at the Laboratory Animal Services research facility at Georgia Regents University and used at the age of 8 weeks. All aspects of the research were conducted in accordance with the guidelines set by the local Institutional Animal Care and Use Committee following an approved protocol.

Biopatterning

Bio-inks were printed as defined patterns on the dermal surface of 5-mm diameter discs of acellular DermaMatrix (ADM) (Synthes, West Chester, PA, USA) using our custom inkjet-based biopatterning system, as previously described [43, 50, 51]. Briefly, the deposited concentrations are modulated using an overprinting strategy whereby each location on the pattern is overprinted with dilute bioinks (sodium phosphate buffer, pH 7.4) such that the deposited concentrations increase in proportion to the number of overprinted drops. Deposited inks absorb into the ADM prior to drying, thus patterns are created within the matrix. A semicircular pattern of growth factor(s) was printed on each disc. Each pattern consisted of recombinant human SDF-1β, BMP-2, BMP-2 + SDF-1β, TGF-β1, or TGF-β1 +

SDF-1β. The BMP-2 and SDF-1β (Peprotech, Rocky Hill, NJ, USA) patterns were printed with 50 overprints (OPs) of 100 μg/ml bioinks, for a total of 108.5 ng of bound growth factor per pattern. rhTGF-β1 (Peprotech) patterns were printed with 30 OPs, for a cumulative total of 65.1 ng of applied growth factor. Notches were cut in the discs opposite the printed area to maintain orientation upon implantation (Fig. 1A).

Experiments and study groups

Animals were assigned randomly to one of 6 treatment groups, saline/vehicle control, SDF-1β, BMP-2, BMP-2+SDF-1β, TGF-β1, and TGF-β1+SDF-1β. The control group had a sample size of n=3, all other groups had n=4.

Mouse calvarial critical size defect model

An established mouse calvarial critical size defect (CSD) model was used to test the ability of the printed growth factors to heal the bony wound [50, 52-54]. Briefly, the mice were anesthetized and the scalps were shaved and sterilized before surgery. A midline scalp incision was used to expose the periosteum. The periosteum overlying the planned craniectomy defect was excised. Under surgical loupes, a 5-mm craniectomy defect was trephinated in the midline of the parietal bones using a slow-speed hand drill. Meticulous care was taken to ensure that underlying dura was not disturbed. Each craniectomy defect was filled with a printed disc prepared with the assigned treatment as above, with orientation guided by the aforementioned notches allowing for the growth factor printed side to approximate the dura mater (Fig. 1A). The skin was closed with a 6×0 polypropolene suture, and the mice received carprofen (2.5 mg/kg; SC; PRN) for 48 h for postoperative analgesic. The mice were euthanized 4 weeks after surgery, at which point the surgical sites were explanted and subjected to radiographic and micro computed tomography analysis.

Radiographic analysis

Radiographic analysis was performed as described previously [31]. Calvarial specimens were placed in 100-mm cell culture dishes and radiographed using a digital imaging instrument (Faxitron X-Ray, Wheeling, IL, USA) following initial calibration. Percent radiographic bone healing for each defect was estimated using a 5.0-mm region of interest (ROI) and ImageJ software (NIH) (Washington, DC, USA). Using Image J, each 5.0-mm ROI was isolated, subjected to system default binary thresholding (white being new bone, black being defect or lack of bone). After thresholding the ROI was halved and each half was measured for amount of new bone. Ratio of new bone was calculated based on the 1/2 area of a 5mm circle. Percent bone healing measure resulted from the above analysis.

Micro computed tomography

Micro computed tomography (μCT) analysis was performed as described previously [31]. Calvarial specimens were scanned using an *ex vivo* μCT system (Skyscan 1174; Skyscan, Aartlesaar, Belgium). The scanner was equipped with a 50 kV, 800 μA X-ray tube and a 1.3 megapixel CCD coupled to a scintillator. Each sample was placed in a sample holder with the sagittal suture oriented parallel to the image plane and scanned in air using a 0.25-mm aluminum filter, 13-μm isotropic voxels, 1300 ms integration time, 0.5° rotation step, and

frame averaging of 4. For 3-D reconstruction (NRecon software, Skyscan), the grey scale was set from 50 to 140. Standard 3-D morphometric parameters [55] (CTAn software, Skyscan) were determined in the ROI (2.5-mm semi-circle; 100 cuts). Representative 3-D images were created using CTvox software (Skyscan).

Osteogenic differentiation

Osteogenic differentiation was performed as described previously [26]. MC3T3-E1 Subclone 4 (ATCC® CRL-2593™) murine pre-osteoblasts (passage 5) were plated at 5.0×10^3 cells/cm^2 in 12-well plates using normal proliferation medium comprised of alpha Modified Eagle Medium (αMEM; Cellgro, Mediatech, Manassas, VA, USA) supplemented with 10% heat-inactivated fetal bovine serum (FBS; Atlanta Biologicals, Lawrenceville, GA, USA). Starting the next day, cells were incubated in standard osteogenic induction medium comprised of αMEM supplemented with 5% FBS, 0.25 mM ascorbic acid (Sigma-Aldrich, St. Louis, MO, USA), 0.1 μM dexamethasone (Sigma-Aldrich), and 10 mM β-glycerophosphate (Sigma-Aldrich) for 21 d. The medium was supplemented with 100 ng/ml rhSDF-1β, 100 ng/ml rhBMP-2 (Peprotech), 100 ng/ml rhSDF-1β + 100 ng/ml rhBMP-2, 10 ng/ml rhTGF-β1, 100 ng/ml rhSDF-1β + 10 ng/ml rhTGF-β1 (all from Peprotech), or vehicle control. Of note, rhBMP-2 in the respective groups was only supplied for the first 24 h in culture to avoid over-stimulation of osteogenic differentiation [26]. Induction media were exchanged every 3 d.

Bone mineral nodule formation assay

Alizarin Red S (ARS) staining was performed to identify calcium mineral content as described previously [26]. After 21 days in culture, MC3T3-E1 monolayers were washed with PBS and fixed in 3% paraformaldehyde (Sigma-Aldrich) for 30 min. Cells were stained with 40 mM ARS pH 4.1 (Sigma-Aldrich) for 15 min followed by washing with excess dH_2O. Stained monolayers were visualized by scanning the plate using a conventional flatbed scanner (Canon, Melville, NY, USA). For quantitative destaining [56], cells were incubated for 10 min with 10% cetylpyridinium chloride (Sigma-Aldrich). Aliquots were diluted (1:10) with PBS, transferred to a 96-well plate (Nunc, Thermo Fisher Scientific, Waltham, MA, USA), and absorbance was read at 570 nm.

Quantitative reverse transcription-polymerase chain reaction

Cells were treated as above. After 7 days in culture, cells were detached, lysates pelleted and RNA isolated using the Qiagen, RNeasy Plus Kit (Valencia, CA, USA) following standard protocol. An n=3 of samples were pooled for each treatment. Quantity and quality of RNA was assessed using a Spectrophotometer (Nanodrop 1000, Wilmington, DE, USA). All ratios of absorbance at 260 and 280 nm were greater than 2.0. Quantitative reverse transcription-polymerase chain reactions (qRT-PCR) were run using a one-step kit for cDNA synthesis (Quanta Biosciences, Gaithersburg, MD, USA) and gene expression. A master mix was made from nuclease free water, master mix, RT/Rnase inhibitor and commercially prepared Taqman probe/primer sets (Life Technologies, Grand Island, NY, USA; Table 1). Three microliters of RNA were added to the master mix for each gene product for each condition by treatment. Analysis was conducted using the ECO Real Time PCR system (Illumina Inc., San Diego, CA, USA) using the average of duplicates.

Expression data was normalized to 18S expression using the comparative C_T method. Quantitative data was compared by treatment. mRNA expression for bone formation marker genes Runx2, Alp, Osx, Col1a1, Ocn, Msx2, Dlx5 and Twist1 were analyzed. The primer sequences used are listed in Table 1.

Statistical analysis

For percent bone healing measured by Faxitron, resulting μCT measures and quantitative Alizarin Red S data, ANOVA with post-hoc Bonferonni multiple comparisons were utilized to determine differences by group. All data are expressed as means ± SD. Differences were considered statistically significant if $p<0.05$. For quantitative qRT-PCR following standardized methodology [57, 58] we set expression differences compared to control and between groups as likely biologically significant and thus statistically significant if a 2-fold mean change increase or decrease was observed.

Results

Radiographic and μCT analysis

Representative radiographic images of the calvarial CSDs treated with printed ADM (semicircle per treatment) at 4 weeks are shown in Figure 1B-G. Quantitative analysis of the newly formed bone within the craniotomy defect revealed limited bone formation in mice treated with SDF-1β, comparable to vehicle controls (Fig. 2). In contrast, a noticeable increase (~ 3-fold) in BMP-2-induced bone formation was observed relative to controls, which was potentiated with SDF-1β co-delivery (Fig. 2). Treatment with TGF-β1 improved the healing outcomes compared to vehicle controls but did not reach the levels of BMP-2. Co-delivery of TGF-β1 + SDF-1β attenuated bone formation levels seen with TGF-β1 alone (Fig. 2). There was a significant difference in mean healing values by treatment group $p=0.003$. Post-hoc analysis revealed BMP-2 + SDF-1β to have significantly greater bone healing than control ($p=0.010$), SDF-1β ($p=0.025$) and TGF-β1+SDF-1β ($p= 0.011$).

E*x vivo* μCT was then employed to characterize bone formation in more detail. Representative 3-D reconstructions of the calvarial CSDs at 4 weeks post-surgery are depicted in Figure 3. Quantitative analyses of standard 3-D bone morphometric parameters concurred with the radiographic estimate and revealed significantly increased percent bone volume (BV/TV) with BMP-2 treatment alone or in combination with SDF-1β relative to vehicle controls (Fig. 4A). A trend towards potentiating effects of SDF-1β co-delivery on BMP-2 osteoinduction was observed. For BV/TV there was a significant difference by treatment group, $p=0.002$. Post-hoc analyses revealed the same significant differences as Faxitron bone healing analysis, i.e., BMP-2 + SDF-1β had significantly greater bone healing than control ($p=0.019$), SDF-1β ($p=0.008$) and TGF-β1 + SDF-1β ($p=0.015$). Trabecular number (Tb.N) appeared to increase with BMP-2 or BMP-2 + SDF-1β compared to controls (Fig. 4B). There was a significant difference for Tb.N by treatment group, $p<0.001$. Post-hoc comparison revealed BMP-2 treatment to have greater trabecular number than control ($p=0.032$), SDF-1β ($p=0.014$), and TGF-β1 + SDF-1β ($p=0.032$); BMP-2 + SDF-1β had greater trabecular number than control ($p=0.005$), SDF-1β ($p=0.002$), TGF-β1 ($p=0.017$) and TGF-β1 + SDF-1β ($p=0.009$). Trabecular thickness (Tb.Th) appeared to be markedly

reduced in both BMP-2 treated groups relative to vehicle controls (Fig. 4C). For Tb.Th, these data violated the assumption of homogeneity of variance. A reciprocal square data transformation allowed data to meet this assumption. There were no significant differences for Tb.Th by treatment group, p=0.086. Trabecular separation (Tb.Sp) appeared to be decreased with BMP-2 or BMP-2 + SDF-1β compared to controls (Fig. 4D). There was a significant difference for Tb.Sp by treatment, p<0.001. Post-hoc comparison revealed BMP-2 treatment to have significantly less trabecular separation than control (p=0.023), SDF-1β (p=0.002), TGF-β1 (p=0.042), and TGF-β1 + SDF-1β (p=0.006); BMP-2 + SDF-1β had significantly less trabecular separation than control (p=0.008), SDF-1β (p=0.001), TGF-β1 (p=0.014), and TGF-β1+SDF-1β (p=0.002). Increased BV/TV and Tb.N in TGF-β1-treated defects reflected the general trend of enhanced bone formation relative to controls seen with radiographic analysis (Fig. 4A,B). Both Tb.Th and Tb.Sp were decreased with TGF-β1 compared to vehicle controls (Fig. 4C,D). Co-delivery of SDF-1β distinctly reduced the regenerative potential of TGF-β1, as evidenced by decreased BV/TV and Tb.N, and increased Tb.Th and Tb.Sp (Fig. 4). No differences in bone morphometric parameters between SDF-1β and vehicle controls were apparent (Fig. 4).

In vitro osteogenic differentiation

To further investigate the effects of co-delivery of BMP-2 + SDF-1β and TGF-β1 + SDF-1β on osteogenic differentiation *in vitro*, calvarial MC3T3-E1 pre-osteoblasts were cultured for 21 d in induction medium in presence of the same treatments used *in vivo*. Calcium mineral content was assessed using standard Alizarin Red S (ARS) staining (Fig. 5A). There was a significant difference in quantitative ARS values by treatment group, p<0.001. In agreement with both radiographic and μCT analysis, osteogenic differentiation of MC3T3-E1 cells was significantly increased with BMP-2 or BMP-2 + SDF-1β treatment compared to all other groups (p<0.001; Fig. 5B). SDF-1β co-delivery noticeably potentiated BMP-2-induced mineralization of the pre-osteoblasts relative to BMP-2 alone but did not reach significant levels. Contrary to the *in vivo* data, no differences were found between TGF-β1 and TGF-β1+SDF-1β groups at 21 d of osteogenic differentiation (Fig. 5). Supplementing SDF-1β to the induction medium had no effect on MC3T3-E1 osteogenic differentiation, as evidenced by similar ARS level relative to vehicle controls (Fig. 5).

Next, we investigated mRNA expression levels of the key osteogenic markers runt-related transcription factor (Runx) 2, alkaline phosphatase (Alp), osterix (Osx), collagen type 1 alpha 1 (Col1a1), osteocalcin (Ocn), msh homeobox 2 (Msx2), distal less homeobox 5 (Dlx5), and twist 1 (Twist1) during the early stages of MC3T3-E1 osteogenic differentiation (7d). Relative transcript levels for Runx2 (Fig. 6A) suggest treatments of SDF-1β, BMP-2 + SDF-1β, and TGF-β1 to have elevated expression, and TGF-β1 + SDF-1β to have reduced expression. Also note, the relative increase when SDF-1β is combined with BMP-2 and the decrease when SDF-1β is co-delivered with TGF-β1. Relative transcript levels for Alp (Fig. 6B) indicate BMP-2 therapy alone and BMP-2 + SDF-1β co-therapy to have increased expression, and TGF-β1 and TGF-β1 + SDF-1β to have decreased expression. Again, SDF-1β was found to potentiate the effect of BMP-2, but attenuate the effect of TGF-β1. Relative transcript levels of Osx (Fig. 6C) suggest treatments of BMP-2 and BMP-2 + SDF-1β to have elevated expression with SDF-1β enhancing the effect of BMP-2. Relative

transcript levels for Col1a1 (Fig. 6D) indicate treatments of SDF-1β, BMP-2 + SDF-1β, TGF-β1, and TGF-β1 + SDF-1β to have increased expression. Again, note the differential effects of SDF-1β on BMP-2 and TGF-β1 therapies. Relative transcript levels for OCN (Fig. 6E) suggest treatments of BMP-2 and BMP-2 + SDF-1β to have elevated expression, and SDF-1β, TGF-β1 and TGF-β1 + SDF-1β to have reduced expression. SDF-1β co-treatment was found to enhance the effect of BMP-2. Relative transcript levels for Msx2 (Fig. 6F) indicate treatments of BMP-2 and BMP-2 + SDF-1β to have increased expression with SDF-1β potentiating the effect of BMP-2 treatment. Note, however, the relationship for treatments of TGF-β1 and TGF-β1 + SDF-1β combined: TGF-β1 alone decreasing and the combined treatment slightly elevating expression of Msx2. Relative transcript levels for Dlx5 (Fig. 6G) suggest treatments of BMP-2 and BMP-2 + SDF-1β to have elevated expression with SDF-1β synergistically increasing expression when co-delivered with BMP-2. Importantly, the effects of TGF-β1 and TGF-β1 + SDF-1β treatments on Dlx5 appeared to be the opposite compared to Msx2 (Fig. 6F,G). Relative transcript levels for Twist1 (Fig. 6H) suggest all potentially osteogenic treatment groups BMP-2, BMP-2 + SDF-1β, TGF-β1 and TGF-β1 + SDF-1β to slightly decrease Twist1 expression.

Collectively, SDF-1β co-delivery synergistically augmented BMP-2-induced new bone formation but attenuated the regenerative potential of TGF-β1, indicative of an opposing regulatory role of the CXCR4/SDF-1 signaling axis dependent on the TGF-β superfamily co-stimulator.

Discussion

The aim of the present study was to utilize previously described biopatterning technology [43-47] to deliver BMP-2, SDF-1β, TGF-β1, or combinations thereof, to investigate their use as potential co-therapies for healing calvarial CSDs. We tested the hypothesis that SDF-1β co-delivery enhances BMP-2- and TGF-β1-driven osteogenesis both *in vitro* and *in vivo* using a mouse calvarial CSD model. The *in vivo* data show that bioprinted low-dose BMP-2 induces significant new bone formation. TGF-β1 was less effective compared to BMP-2, and SDF-1β did not enhance osteogenesis above vehicle control levels. Co-delivery of BMP-2 + SDF-1β was found to augment BMP-2-induced bone formation compared to BMP-2 alone. In contrast, co-delivery of TGF-β1 + SDF-1β decreased bone healing seen with TGF-β1 alone. This observation was further confirmed *in vitro* by osteogenic differentiation studies using MC3T3-E1 cells.

A major problem in the field of craniofacial surgery is non-healing bony defects. Causes of craniofacial injury include trauma and tumor removal, contributing to prevalent mortality and morbidity [59, 60]. This is further complicated by factors that compromise the recipient wound bed or interfere with optimal healing (e.g., irradiation, infection, surgical damage) [3, 61, 62]. Autologous bone grafts remain the standard of care, although, the process of harvesting is associated with morbidity and a number of complications. Therefore, allogeneic and synthetic bone grafts are often used, despite their disadvantages such as the lack of robust bioactivity, incompatibility, instability, and susceptibility to infection [1]. While BMP-2 therapies address some of these issues, emerging safety concerns have

motivated development of alternative strategies for augmentation of clinical bone healing [63].

Previous studies have suggested that the CXCR4/SDF-1 axis functions in postnatal bone formation by regulating osteoblast development in cooperation with BMP signaling, and that CXCR4 acts as an endogenous signaling component necessary for bone formation [30]. We [26] and others [64] have shown that bone marrow endothelial and stromal cells, and osteoblasts express both major SDF-1 splice variants, and that unexpectedly the beta isoform may be present at a high level in bone tissues [64]. We have also shown that, independent of SDF-1α, SDF-1β enhances BMP-2-stimulated mineralization, mRNA and protein expression of key osteogenic markers, regulates BMP-2 signal transduction via Erk1/2 phosphorylation, and promotes the migratory response of CXCR4-expressing BMSCs *in vitro* [26], suggesting both SDF-1β autocrine and paracrine activity. An important characteristic of SDF-1β is its protection from proteolytic cleavage at the C-terminus, distinguishing SDF-1β from SDF-1α. Further, the four additional C-terminal amino acids are thought to mediate SDF-1β cell and extracellular stability, increasing its half-life and potency in vascularized tissues [1, 48, 49]. This suggests that SDF-1, in particular the beta isoform, is of interest in translational approaches to enhance bone formation via the BMP-2 pathway, as recently reported [31], and may permit low-dose clinical BMP-2 therapies with reduced negative side effects [8, 65]

Our *in vivo* data, obtained using the established CSD [50, 52-54], suggest that biopatterned BMP-2 at a low-dose induces significant new bone formation, while TGF-β1 only moderately improved the outcome. SDF-1β does not induce osteogenesis, as evidenced by comparable levels of bone formation to vehicle controls. Importantly, BMP-2 + SDF-1β co-therapy was found to augment BMP-2-induced bone formation, thereby confirming previous findings from our group across species (rat vs. mouse) and delivery technologies (absorbable collagen sponge (ACS) vs. ADM; soak-loaded vs. bioprinted) [31]. To that end, it is critical to point out that the BMP-2 dose printed on ADM (11.1 ng/mm^2) used in this study was comparable to the suboptimal BMP-2 dose soak-loaded on ACS (9.9 ng/mm^2) previously described [31]. Despite the similar absolute BMP-2 dose per matrix/defect, the observed outcomes were distinctly different. While we found robust osteoinduction using the biopatterned low-dose BMP-2 on ADM, no significant bone formation was apparent using the suboptimal soak-loaded BMP-2 on ACS in the rat model after the same 4-week healing interval [31]. These observations can be extended with respect to the SDF-1β doses used in both studies. SDF-1β was printed here on ADM at the same 11.1 ng/mm^2, which significantly enhanced the osteoinductive properties of low-dose BMP-2. In contrast, the therapeutic dose range of SDF-1β co-delivered with suboptimal BMP-2 dose far exceeded the bioprinted SDF-1β dose (298.2-1192.8 ng/mm^2; 27-107-fold increased) [31]. This suggests that the biopatterning technology allows for the use of very low therapeutic doses of BMP-2 and SDF-1β in the nanogram range, validating previous reports [31, 50, 54]. With regard to the release kinetics of the biopatterned cytokines, our group has previously reported that after 24 h of incubation in standard cell culture medium at 37°C, ~80% of the biopatterned BMP-2 remained bound to the ADM with subsequent slow release over 14 days such that ~70% of bound BMP-2 remained [54]. Therefore, the retention of

biopatterned BMP-2 on ADM appears to be significantly longer than what is generally reported for soak-loaded BMP-2 on ACS. A recent study showed that only ~20% of the soak-loaded BMP-2 remains bound to the ACS after 6 d *in vitro* [66]. Comparable short retention times have been described *in vivo* using both ectopic (6 d; ~10%) [67] and orthotopic (7 d; ~30%) [68] bone formation models. Collectively, the inkjet-based biopatterning technology combined with the ADM delivery system may protect the printed cytokines until solubilized, and allow a prolonged retention and an extended bioavailability compared to other technologies.

A key component of this study was the inclusion of another TGF-β superfamily member, TGF-β1, used as stand-alone as well as combination therapy. TGF-β1 regulates cell proliferation and migration of different cell types, including osteoblasts. Therefore, TGF-β1 has osteogenic properties [32, 33]. TGF-β1 is expressed constitutively in healing bone fractures and is involved in bone formation by stimulating Runx2 [34-39]. In agreement with this, we observed enhanced bone formation using biopatterned TGF-β1 compared to vehicle controls. Unexpectedly, co-delivery of TGF-β1 + SDF-1β attenuated the therapeutic effects of TGF-β1 *in vivo*. We further confirmed these relationships between the cytokines *in vitro* by standard Alizarin Red S (ARS) staining of mineralization and transcript analyses of key osteogenic markers in murine calvarial MC3T3-E1 pre-osteoblasts. ARS staining for calcified nodules at 21 d was generally in agreement with the *in vivo* findings, although the reduction in mineralization with co-delivery of TGF-β1 + SDF-1β compared to TGF-β1 alone was less pronounced.

Consistent with the expression of BMP and TGF-β receptors in mesenchymal cells and osteoblasts, both BMP-2 and TGF-β1 regulate osteogenic differentiation albeit using different signal transduction pathways. Several transcription factors are sequentially expressed during BMP-induced osteoblast differentiation and are required for cell maturation. Among these, Runx2 and Osx are considered master switches in osteoblastogenesis, which can directly be upregulated by BMPs and subsequently activate downstream genes necessary for the osteoblast phenotype such as Col1a1 and Ocn [69]. The expression of Msx2 is rapidly induced in response to BMP-2, which plays an important role in promoting osteoblast commitment [70], as evidenced by Msx2 directly targeting Ocn [71]. Furthermore, Msx2 has been suggested to inhibit Dlx5 regulation of BMP-2-mediated osteogenesis and inhibit osteoblast differentiation [39, 69]. Dlx5 is specifically expressed in differentiating osteoblasts and binds the Runx2 promoter to confer BMP-2 osteoinduction [39]. Our data suggest that SDF-1β co-delivery enhances BMP-2-induced expression of Runx2, Alp, Osx, Col1a1, Ocn, Msx2, and Dlx5 in pre-osteoblasts relative to BMP-2 alone, confirming previous findings from our group using mesenchymal stem cells [26]. We also observed down-regulation of Twist1 for all cell treatments with the exception of SDF-1β alone. This is a confirmatory finding for the maturation of the pre-osteoblasts toward their final phenotype as Twist is a marker of stemness of cells [72]. In contrast, SDF-1β appears to act to limit further differentiation decreasing Runx2 expression when co-delivered with TGF-β1 compared to TGF-β1 administration alone. This appears to result in less Alp, Col1a1, and Dlx5 expression. Although possibly not biologically significant (within ± 2-fold change), we found opposing patterns of Msx2 and Dlx5 expression suggesting a potential

role for SDF-1β in contextually eliciting differential effects on the expression of these important transcription factors. Taken together, we observe what might represent a rescue effect with reference to late stage differentiation, specifically Ocn expression. TGF-β1 has previously been shown to inhibit late stage differentiation, an effect we confirmed here *in vitro* [39, 69]. It may be that setting up the healing axis and inhibition of early Runx2 expression with TGF-β1 + SDF-1β co-treatment may underlie our observed outcome of reduced healing. However, we can only speculate on the detailed molecular pathways involved, this points to future areas of investigation.

Collectively, our data suggest that SDF-1β co-therapy synergistically augments BMP-2-induced new bone formation but attenuates the regenerative potential of TGF-β1, indicative of an opposing regulatory role of the CXCR4/SDF-1 signaling axis dependent on the TGF-β superfamily co-stimulator. Given the numerous adverse effects reported with current commercial high-dose BMP-2 products, including significant inflammatory and immunogenic responses [8, 65], the opportunities to significantly reduce the locally applied BMP-2 dose for bone regeneration using biopatterning technology presents an intriguing avenue for translational development.

Conclusion

SDF-1β enhances BMP-2-driven osteogenesis and bone healing in a mouse critical size calvarial defect model. It does not, however, improve healing utilizing a TGF-β1 based therapy. SDF-1β augments the positive effects BMP-2 has on osteogenic gene expression but reduces those same positive effects for TGF-β1. This relationship between SDF-1β and opposing effects on different members of the TGF-β superfamily necessitates further investigation to determine what downstream targets are affected by SDF-1β and how this translates to differences in bony healing and if it contributes to clinical impaired healing, i.e. in diabetes or aging.

Acknowledgments

This study was supported by a grant from the Musculoskeletal Transplant Foundation (JC), by the Institute for Regenerative and Reparative Medicine at Georgia Regents University (JC) and the Department of Veterans Affairs VA104462(WDH), the National Institute of Health, National Institute of Aging NIH-NIA PO1-AG036675 (WDH). Authors would like to thank Mr. Kameron Khaksarfard for his help with this study. The contents of this publication do not represent the views of the Department of Veterans Affairs, or the United States Government.

Abbreviations

BMP-2	bone morphogenetic protein-2
SDF-1β	stromal cell-derived factor-1β
TGF-β1	transforming growth factor-β1
ADM	acellular DermaMatrix
CSD	critical size defect

References

[1]. De La Luz Sierra M, Yang F, Narazaki M, Salvucci O, Davis D, Yarchoan R, Zhang HH, Fales H, Tosato G. Differential processing of stromal-derived factor-1alpha and stromal-derived factor-1beta explains functional diversity. Blood. 2004; 103:2452–9. [PubMed: 14525775]

[2]. Cowan CM, Aalami OO, Shi YY, Chou YF, Mari C, Thomas R, Quarto N, Nacamuli RP, Contag CH, Wu B, Longaker MT. Bone morphogenetic protein 2 and retinoic acid accelerate in vivo bone formation, osteoclast recruitment, and bone turnover. Tissue Eng. 2005; 11:645–58. [PubMed: 15869441]

[3]. Smith DM, Cooper GM, Mooney MP, Marra KG, Losee JE. Bone morphogenetic protein 2 therapy for craniofacial surgery. J Craniofac Surg. 2008; 19:1244–59. [PubMed: 18812847]

[4]. Sen MK, Miclau T. Autologous iliac crest bone graft: should it still be the gold standard for treating nonunions? Injury. 2007; 38(Suppl 1):S75–80. [PubMed: 17383488]

[5]. David L, Argenta L, Fisher D. Hydroxyapatite cement in pediatric craniofacial reconstruction. J Craniofac Surg. 2005; 16:129–33. [PubMed: 15699660]

[6]. Crawford CH 3rd, Seligson D. Atrophic nonunion of humeral diaphysis treated with locking plate and recombinant bone morphogenetic protein: nine cases. Am J Orthop (Belle Mead NJ). 2009; 38:567–70. [PubMed: 20049351]

[7]. De Long WG Jr. Einhorn TA, Koval K, McKee M, Smith W, Sanders R, Watson T. Bone grafts and bone graft substitutes in orthopaedic trauma surgery. A critical analysis. J Bone Joint Surg Am. 2007; 89:649–58. [PubMed: 17332116]

[8]. Govender S, Csimma C, Genant HK, Valentin-Opran A, Amit Y, Arbel R, Aro H, Atar D, Bishay M, Borner MG, Chiron P, Choong P, Cinats J, Courtenay B, Feibel R, et al. Recombinant human bone morphogenetic protein-2 for treatment of open tibial fractures: a prospective, controlled, randomized study of four hundred and fifty patients. J Bone Joint Surg Am. 2002; 84-A:2123–34. [PubMed: 12473698]

[9]. Johnson EE, Urist MR. Human bone morphogenetic protein allografting for reconstruction of femoral nonunion. Clin Orthop Relat Res. 2000:61–74. [PubMed: 10693551]

[10]. McKay WF, Peckham SM, Badura JM. A comprehensive clinical review of recombinant human bone morphogenetic protein-2 (INFUSE Bone Graft). Int Orthop. 2007; 31:729–34. [PubMed: 17639384]

[11]. Swiontkowski MF, Aro HT, Donell S, Esterhai JL, Goulet J, Jones A, Kregor PJ, Nordsletten L, Paiement G, Patel A. Recombinant human bone morphogenetic protein-2 in open tibial fractures. A subgroup analysis of data combined from two prospective randomized studies. J Bone Joint Surg Am. 2006; 88:1258–65. [PubMed: 16757759]

[12]. White AP, Vaccaro AR, Hall JA, Whang PG, Friel BC, McKee MD. Clinical applications of BMP-7/OP-1 in fractures, nonunions and spinal fusion. Int Orthop. 2007; 31:735–41. [PubMed: 17962946]

[13]. Bess S, Line BG, Boachie-Adjei O, Hart R, Lafage V, Schwab F, Akbarnia BA, Ames CP, Burton DC, Hostin RA, Klineberg E, Mundis G, Shaffrey CI, Smith JS. 140 Does Recombinant Human Bone Morphogenetic Protein-2 (BMP) Use in Adult Spinal Deformity (ASD) Increase Complications and Are Complications Dose Related? A Prospective, Multicenter Study of 257 Consecutive Patients. Neurosurgery. 2012; 71:E556–7.

[14]. Hodges SD, Eck JC, Newton D. Retrospective study of posterior cervical fusions with rhBMP-2. Orthopedics. 2012; 35:e895–8. [PubMed: 22691663]

[15]. He D, Genecov DG, Herbert M, Barcelo R, Elsalanty ME, Weprin BE, Opperman LA. Effect of recombinant human bone morphogenetic protein-2 on bone regeneration in large defects of the growing canine skull after dura mater replacement with a dura mater substitute. J Neurosurg. 2009; 112:319–28. [PubMed: 19267528]

[16]. Smith DM, Afifi AM, Cooper GM, Mooney MP, Marra KG, Losee JE. BMP-2-based repair of large-scale calvarial defects in an experimental model: regenerative surgery in cranioplasty. J Craniofac Surg. 2008; 19:1315–22. [PubMed: 18812857]

[17]. Zlotnik A, Yoshie O. Chemokines: a new classification system and their role in immunity. Immunity. 2000; 12:121–7. [PubMed: 10714678]

[18]. Bleul CC, Farzan M, Choe H, Parolin C, Clark-Lewis I, Sodroski J, Springer TA. The lymphocyte chemoattractant SDF-1 is a ligand for LESTR/fusin and blocks HIV-1 entry. Nature. 1996; 382:829–33. [PubMed: 8752280]

[19]. Feng Y, Broder CC, Kennedy PE, Berger EA. HIV-1 entry cofactor: functional cDNA cloning of a seven-transmembrane, G protein-coupled receptor. Science. 1996; 272:872–7. [PubMed: 8629022]

[20]. Heesen M, Berman MA, Benson JD, Gerard C, Dorf ME. Cloning of the mouse fusin gene, homologue to a human HIV-1 co-factor. J Immunol. 1996; 157:5455–60. [PubMed: 8955194]

[21]. Granero-Molto F, Weis JA, Miga MI, Landis B, Myers TJ, O'Rear L, Longobardi L, Jansen ED, Mortlock DP, Spagnoli A. Regenerative effects of transplanted mesenchymal stem cells in fracture healing. Stem Cells. 2009; 27:1887–98. [PubMed: 19544445]

[22]. Kitaori T, Ito H, Schwarz EM, Tsutsumi R, Yoshitomi H, Oishi S, Nakano M, Fujii N, Nagasawa T, Nakamura T. Stromal cell-derived factor 1/CXCR4 signaling is critical for the recruitment of mesenchymal stem cells to the fracture site during skeletal repair in a mouse model. Arthritis Rheum. 2009; 60:813–23. [PubMed: 19248097]

[23]. Otsuru S, Tamai K, Yamazaki T, Yoshikawa H, Kaneda Y. Circulating bone marrow-derived osteoblast progenitor cells are recruited to the bone-forming site by the CXCR4/stromal cell-derived factor-1 pathway. Stem Cells. 2008; 26:223–34. [PubMed: 17932420]

[24]. Hosogane N, Huang Z, Rawlins BA, Liu X, Boachie-Adjei O, Boskey AL, Zhu W. Stromal derived factor-1 regulates bone morphogenetic protein 2-induced osteogenic differentiation of primary mesenchymal stem cells. Int J Biochem Cell Biol. 2010; 42:1132–41. [PubMed: 20362069]

[25]. Zhu W, Boachie-Adjei O, Rawlins BA, Frenkel B, Boskey AL, Ivashkiv LB, Blobel CP. A novel regulatory role for stromal-derived factor-1 signaling in bone morphogenic protein-2 osteogenic differentiation of mesenchymal C2C12 cells. Journal of Biological Chemistry. 2007; 282:18676–85. [PubMed: 17439946]

[26]. Herberg S, Fulzele S, Yang N, Shi X, Hess M, Periyasamy-Thandavan S, Hamrick MW, Isales CM, Hill WD. Stromal cell-derived factor-1beta potentiates bone morphogenetic protein-2-stimulated osteoinduction of genetically engineered bone marrow-derived mesenchymal stem cells in vitro. Tissue Eng Part A. 2013; 19:1–13. [PubMed: 22779446]

[27]. Higashino K, Viggeswarapu M, Bargouti M, Liu H, Titus L, Boden SD. Stromal cell-derived factor-1 potentiates bone morphogenetic protein-2 induced bone formation. Tissue Engineering. Part A. 2011; 17:523–30. [PubMed: 21043834]

[28]. Wise JK, Sumner DR, Virdi AS. Modulation of stromal cell-derived factor-1/CXC chemokine receptor 4 axis enhances rhBMP-2-induced ectopic bone formation. Tissue Eng Part A. 2012; 18:860–9. [PubMed: 22035136]

[29]. Ratanavaraporn J, Furuya H, Kohara H, Tabata Y. Synergistic effects of the dual release of stromal cell-derived factor-1 and bone morphogenetic protein-2 from hydrogels on bone regeneration. Biomaterials. 2011; 32:2797–811. [PubMed: 21257197]

[30]. Zhu W, Liang G, Huang Z, Doty SB, Boskey AL. Conditional inactivation of the CXCR4 receptor in osteoprecursors reduces postnatal bone formation due to impaired osteoblast development. J Biol Chem. 2011; 286:26794–805. [PubMed: 21636574]

[31]. Herberg S, Susin C, Pelaez M, Howie RN, Moreno de Freitas R, Lee J, Cray JJ Jr. Johnson MH, Elsalanty ME, Hamrick MW, Isales CM, Wikesjo UM, Hill WD. Low-dose bone morphogenetic protein-2/stromal cell-derived factor-1beta cotherapy induces bone regeneration in critical-size rat calvarial defects. Tissue Eng Part A. 2014; 20:1444–53. [PubMed: 24341891]

[32]. Capron C, Lacout C, Lecluse Y, Jalbert V, Chagraoui H, Charrier S, Galy A, Bennaceur-Griscelli A, Cramer-Borde E, Vainchenker W. A major role of TGF-beta1 in the homing capacities of murine hematopoietic stem cell/progenitors. Blood. 2010; 116:1244–53. [PubMed: 20489054]

[33]. Tzakas P, Wong BY, Logan AG, Rubin LA, Cole DE. Transforming growth factor beta-1 (TGFB1) and peak bone mass: association between intragenic polymorphisms and quantitative ultrasound of the heel. BMC Musculoskelet Disord. 2005; 6:29. [PubMed: 15955247]

[34]. Bonewald LF, Dallas SL. Role of active and latent transforming growth factor beta in bone formation. J Cell Biochem. 1994; 55:350–7. [PubMed: 7962167]

[35]. Centrella M, Horowitz MC, Wozney JM, McCarthy TL. Transforming growth factor-beta gene family members and bone. Endocr Rev. 1994; 15:27–39. [PubMed: 8156937]

[36]. Cho TJ, Gerstenfeld LC, Einhorn TA. Differential temporal expression of members of the transforming growth factor beta superfamily during murine fracture healing. J Bone Miner Res. 2002; 17:513–20. [PubMed: 11874242]

[37]. Lee KS, Kim HJ, Li QL, Chi XZ, Ueta C, Komori T, Wozney JM, Kim EG, Choi JY, Ryoo HM, Bae SC. Runx2 is a common target of transforming growth factor beta1 and bone morphogenetic protein 2, and cooperation between Runx2 and Smad5 induces osteoblast-specific gene expression in the pluripotent mesenchymal precursor cell line C2C12. Mol Cell Biol. 2000; 20:8783–92. [PubMed: 11073979]

[38]. Lee MH, Javed A, Kim HJ, Shin HI, Gutierrez S, Choi JY, Rosen V, Stein JL, van Wijnen AJ, Stein GS, Lian JB, Ryoo HM. Transient upregulation of CBFA1 in response to bone morphogenetic protein-2 and transforming growth factor beta1 in C2C12 myogenic cells coincides with suppression of the myogenic phenotype but is not sufficient for osteoblast differentiation. J Cell Biochem. 1999; 73:114–25. [PubMed: 10088730]

[39]. Lee MH, Kim YJ, Kim HJ, Park HD, Kang AR, Kyung HM, Sung JH, Wozney JM, Kim HJ, Ryoo HM. BMP-2-induced Runx2 expression is mediated by Dlx5, and TGF-beta 1 opposes the BMP-2-induced osteoblast differentiation by suppression of Dlx5 expression. J Biol Chem. 2003; 278:34387–94. [PubMed: 12815054]

[40]. Spinella-Jaegle S, Roman-Roman S, Faucheu C, Dunn FW, Kawai S, Gallea S, Stiot V, Blanchet AM, Courtois B, Baron R, Rawadi G. Opposite effects of bone morphogenetic protein-2 and transforming growth factor-beta1 on osteoblast differentiation. Bone. 2001; 29:323–30. [PubMed: 11595614]

[41]. Hasegawa T, Chosa N, Asakawa T, Yoshimura Y, Fujihara Y, Kitamura T, Tanaka M, Ishisaki A, Mitome M. Differential effects of TGF-beta1 and FGF-2 on SDF-1alpha expression in human periodontal ligament cells derived from deciduous teeth in vitro. Int J Mol Med. 2012; 30:35–40. [PubMed: 22469823]

[42]. Chim H, Miller E, Gliniak C, Alsberg E. Stromal-cell-derived factor (SDF) 1-alpha in combination with BMP-2 and TGF-beta1 induces site-directed cell homing and osteogenic and chondrogenic differentiation for tissue engineering without the requirement for cell seeding. Cell Tissue Res. 2012

[43]. Miller ED, Phillippi JA, Fisher GW, Campbell PG, Walker LM, Weiss LE. Inkjet printing of growth factor concentration gradients and combinatorial arrays immobilized on biologically-relevant substrates. Combinatorial chemistry & high throughput screening. 2009; 12:604–18. [PubMed: 19601758]

[44]. Campbell PG, Weiss LE. Tissue engineering with the aid of inkjet printers. Expert opinion on biological therapy. 2007; 7:1123–7. [PubMed: 17696812]

[45]. Miller ED, Fisher GW, Weiss LE, Walker LM, Campbell PG. Dose-dependent cell growth in response to concentration modulated patterns of FGF-2 printed on fibrin. Biomaterials. 2006; 27:2213–21. [PubMed: 16325254]

[46]. Campbell PG, Miller ED, Fisher GW, Walker LM, Weiss LE. Engineered spatial patterns of FGF-2 immobilized on fibrin direct cell organization. Biomaterials. 2005; 26:6762–70. [PubMed: 15941581]

[47]. Cooper GM, Miller ED, Decesare GE, Usas A, Lensie EL, Bykowski MR, Huard J, Weiss LE, Losee JE, Campbell PG. Inkjet-based biopatterning of bone morphogenetic protein-2 to spatially control calvarial bone formation. Tissue Eng Part A. 2010; 16:1749–59. [PubMed: 20028232]

[48]. Davis DA, Singer KE, De La Luz Sierra M, Narazaki M, Yang F, Fales HM, Yarchoan R, Tosato G. Identification of carboxypeptidase N as an enzyme responsible for C-terminal cleavage of stromal cell-derived factor-1alpha in the circulation. Blood. 2005; 105:4561–8. [PubMed: 15718415]

[49]. Marquez-Curtis L, Jalili A, Deiteren K, Shirvaikar N, Lambeir AM, Janowska-Wieczorek A. Carboxypeptidase M expressed by human bone marrow cells cleaves the C-terminal lysine of stromal cell-derived factor-1alpha: another player in hematopoietic stem/progenitor cell mobilization? Stem Cells. 2008; 26:1211–20. [PubMed: 18292211]

[50]. Smith DM, Cray JJ Jr. Weiss LE, Dai Fei EK, Shakir S, Rottgers SA, Losee JE, Campbell PG, Cooper GM. Precise control of osteogenesis for craniofacial defect repair: the role of direct osteoprogenitor contact in BMP-2-based bioprinting. Annals of plastic surgery. 2012; 69:485–8. [PubMed: 22972553]

[51]. Cooper GM, Miller ED, Decesare GE, Usas A, Lensie EL, Bykowski MR, Huard J, Weiss LE, Losee JE, Campbell PG. Inkjet-based biopatterning of bone morphogenetic protein-2 to spatially control calvarial bone formation. Tissue engineering. Part A. 2010; 16:1749–59. [PubMed: 20028232]

[52]. Hollinger JO, Kleinschmidt JC. The critical size defect as an experimental model to test bone repair materials. J Craniofac Surg. 1990; 1:60–8. [PubMed: 1965154]

[53]. Schmitz JP, Hollinger JO. The critical size defect as an experimental model for craniomandibulofacial nonunions. Clinical Orthopaedics and Related Research. 1986:299–308. [PubMed: 3084153]

[54]. Cooper GM, Mooney MP, Gosain AK, Campbell PG, Losee JE, Huard J. Testing the critical size in calvarial bone defects: revisiting the concept of a critical-size defect. Plastic and reconstructive surgery. 2010; 125:1685–92. [PubMed: 20517092]

[55]. Bouxsein ML, Boyd SK, Christiansen BA, Guldberg RE, Jepsen KJ, Muller R. Guidelines for assessment of bone microstructure in rodents using micro-computed tomography. J Bone Miner Res. 2010; 25:1468–86. [PubMed: 20533309]

[56]. Ripoll CB, Bunnell BA. Comparative characterization of mesenchymal stem cells from eGFP transgenic and non-transgenic mice. BMC Cell Biol. 2009; 10:3. [PubMed: 19144129]

[57]. Cray JJ Jr. Khaksarfard K, Weinberg SM, Elsalanty M, Yu JC. Effects of thyroxine exposure on osteogenesis in mouse calvarial pre-osteoblasts. PloS one. 2013; 8:e69067. [PubMed: 23935926]

[58]. Morey JS, Ryan JC, Van Dolah FM. Microarray validation: factors influencing correlation between oligonucleotide microarrays and real-time PCR. Biological procedures online. 2006; 8:175–93. [PubMed: 17242735]

[59]. Burt CW, Fingerhut LA. Injury visits to hospital emergency departments: United States, 1992-95. Vital Health Stat. 1998; 13:1–76.

[60]. Mitchener TA, Canham-Chervak M. Oral-maxillofacial injury surveillance in the Department of Defense, 1996-2005. Am J Prev Med. 2010; 38:S86–93. [PubMed: 20117604]

[61]. DeCesare GE, Cooper GM, Smith DM, Cray JJ Jr. Durham EL, Kinsella CR Jr. Mooney MP, Losee JE. Novel animal model of calvarial defect in an infected unfavorable wound: reconstruction with rhBMP-2. Plastic and reconstructive surgery. 2011; 127:588–94. [PubMed: 21285763]

[62]. Kinsella CR Jr. Bykowski MR, Lin AY, Cray JJ, Durham EL, Smith DM, DeCesare GE, Mooney MP, Cooper GM, Losee JE. BMP-2-mediated regeneration of large-scale cranial defects in the canine: an examination of different carriers. Plastic and reconstructive surgery. 2012; 127:1865–73. [PubMed: 21532416]

[63]. Carragee EJ, Hurwitz EL, Weiner BK. A critical review of recombinant human bone morphogenetic protein-2 trials in spinal surgery: emerging safety concerns and lessons learned. Spine J. 2011; 11:471–91. [PubMed: 21729796]

[64]. Katayama Y, Battista M, Kao WM, Hidalgo A, Peired AJ, Thomas SA, Frenette PS. Signals from the sympathetic nervous system regulate hematopoietic stem cell egress from bone marrow. Cell. 2006; 124:407–21. [PubMed: 16439213]

[65]. Boerckel JD, Kolambkar YM, Dupont KM, Uhrig BA, Phelps EA, Stevens HY, Garcia AJ, Guldberg RE. Effects of protein dose and delivery system on BMP-mediated bone regeneration. Biomaterials. 2011; 32:5241–51. [PubMed: 21507479]

[66]. Yang HS, La WG, Cho YM, Shin W, Yeo GD, Kim BS. Comparison between heparin-conjugated fibrin and collagen sponge as bone morphogenetic protein-2 carriers for bone regeneration. Exp Mol Med. 2012; 44:350–5. [PubMed: 22322342]

[67]. Friess W, Uludag H, Foskett S, Biron R, Sargeant C. Characterization of absorbable collagen sponges as rhBMP-2 carriers. Int J Pharm. 1999; 187:91–9. [PubMed: 10502616]

[68]. Geiger M, Li RH, Friess W. Collagen sponges for bone regeneration with rhBMP-2. Adv Drug Deliv Rev. 2003; 55:1613–29. [PubMed: 14623404]

[69]. Ryoo HM, Lee MH, Kim YJ. Critical molecular switches involved in BMP-2-induced osteogenic differentiation of mesenchymal cells. Gene. 2006; 366:51–7. [PubMed: 16314053]

[70]. Brugger SM, Merrill AE, Torres-Vazquez J, Wu N, Ting MC, Cho JY, Dobias SL, Yi SE, Lyons K, Bell JR, Arora K, Warrior R, Maxson R. A phylogenetically conserved cis-regulatory module in the Msx2 promoter is sufficient for BMP-dependent transcription in murine and Drosophila embryos. Development. 2004; 131:5153–65. [PubMed: 15459107]

[71]. Bidder M, Latifi T, Towler DA. Reciprocal temporospatial patterns of Msx2 and Osteocalcin gene expression during murine odontogenesis. J Bone Miner Res. 1998; 13:609–19. [PubMed: 9556061]

[72]. Miraoui H, Marie PJ. Pivotal role of Twist in skeletal biology and pathology. Gene. 2010; 468:1–7. [PubMed: 20696219]

Highlights

We biopattern low doses of BMP-2, SDF-1β, TGF-β1 or combinations on DermaMatrix.

We assess bone healing in a critical size mouse calvarial defect model at 4 weeks.

BMP-2 induced greater bone healing than TGF-β1. SDF-1β was comparable to controls.

BMP-2+SDF-1β augmented BMP-2-induced bone healing.

TGF-β1+SDF-1β attenuated TGF-β1-induced bone healing.

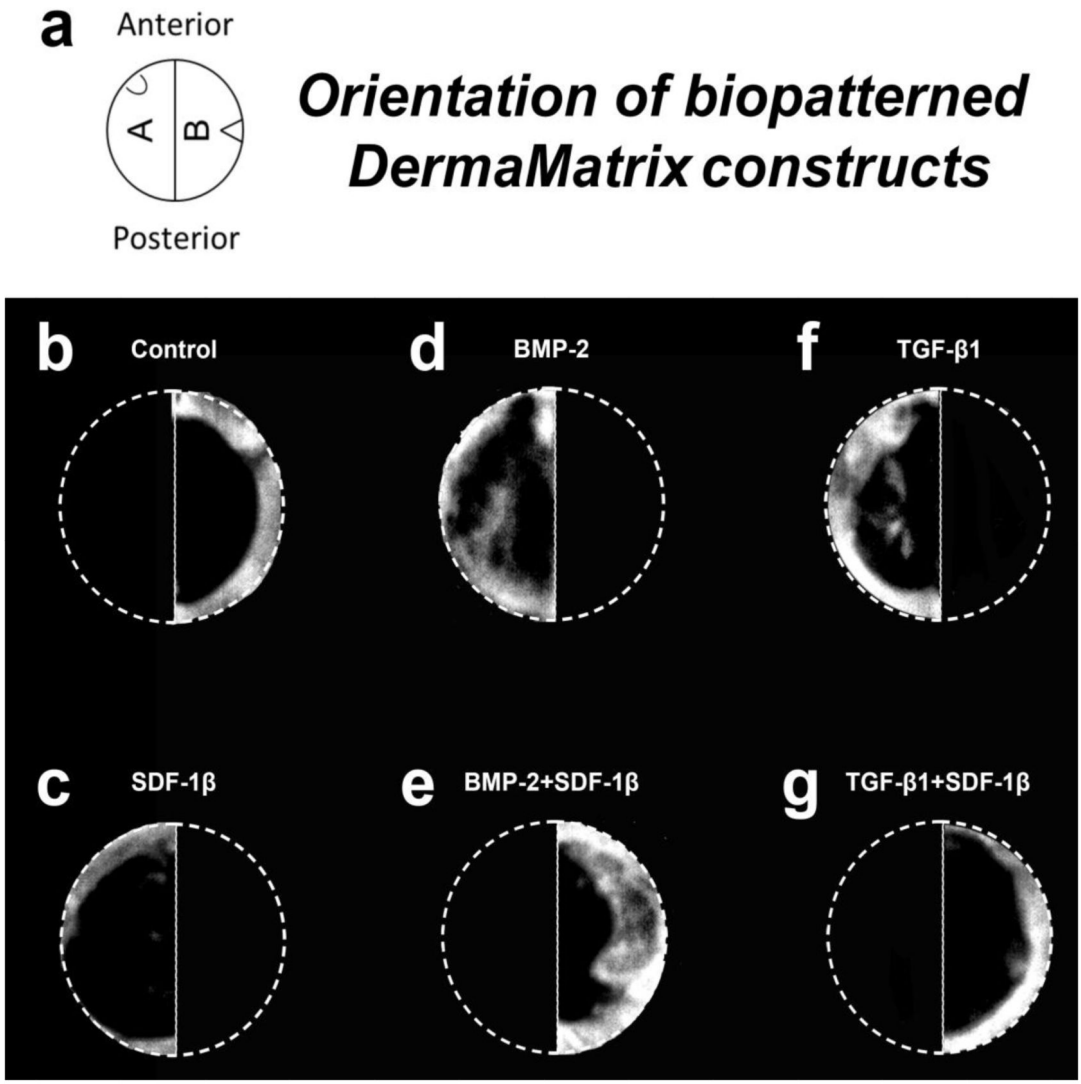

Figure 1.

Representative radiographs for each group, 4 weeks post-op. a-Diagram of the bioprinted matrices. Note the notches used for orientation, b-Control, c-SDF-1β, d-BMP-2, e-BMP-2+SDF-1β, f-TGF-β1, g-TGF-β1+SDF-1β.

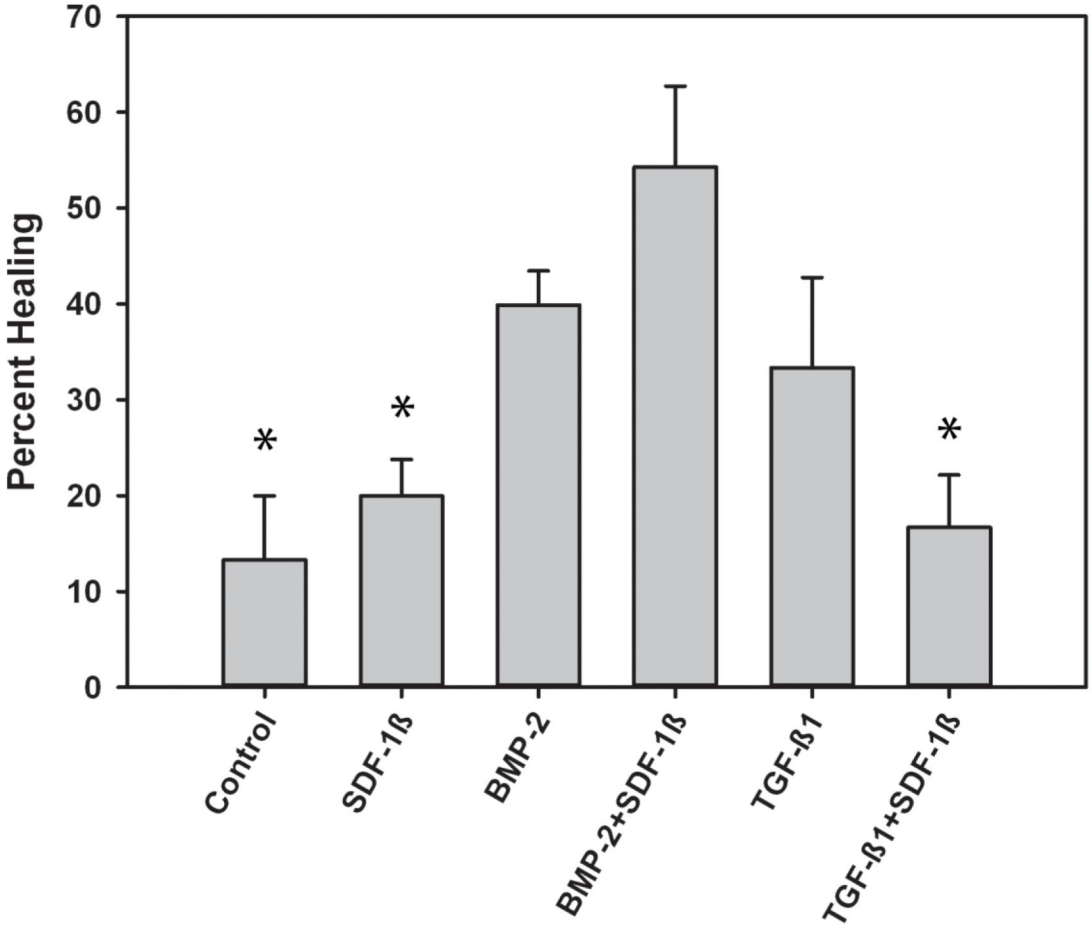

Figure 2.

Mean percent healing of CSD by cytokine treatment, 4 weeks post-op. * indicates significant difference compared to *BMP-2+SDF-1β* group

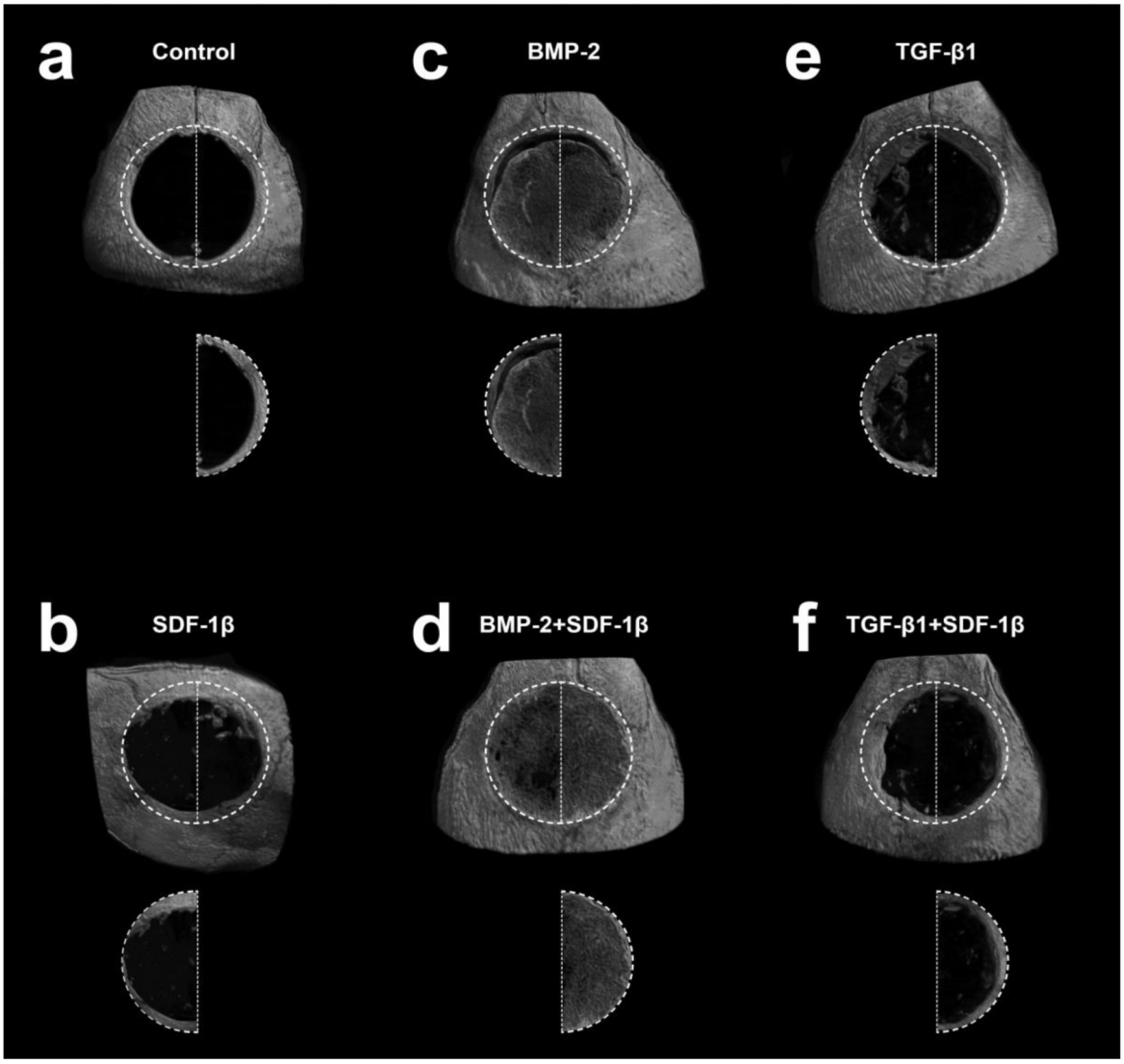

Figure 3.

Representative 3-D reconstruction of μCT images for each group, 4 weeks post-op. a-Control, b-SDF-1β, c-BMP-2, d-BMP-2+SDF-1β, e-TGF-β1, f-TGF-β1+SDF-1β.

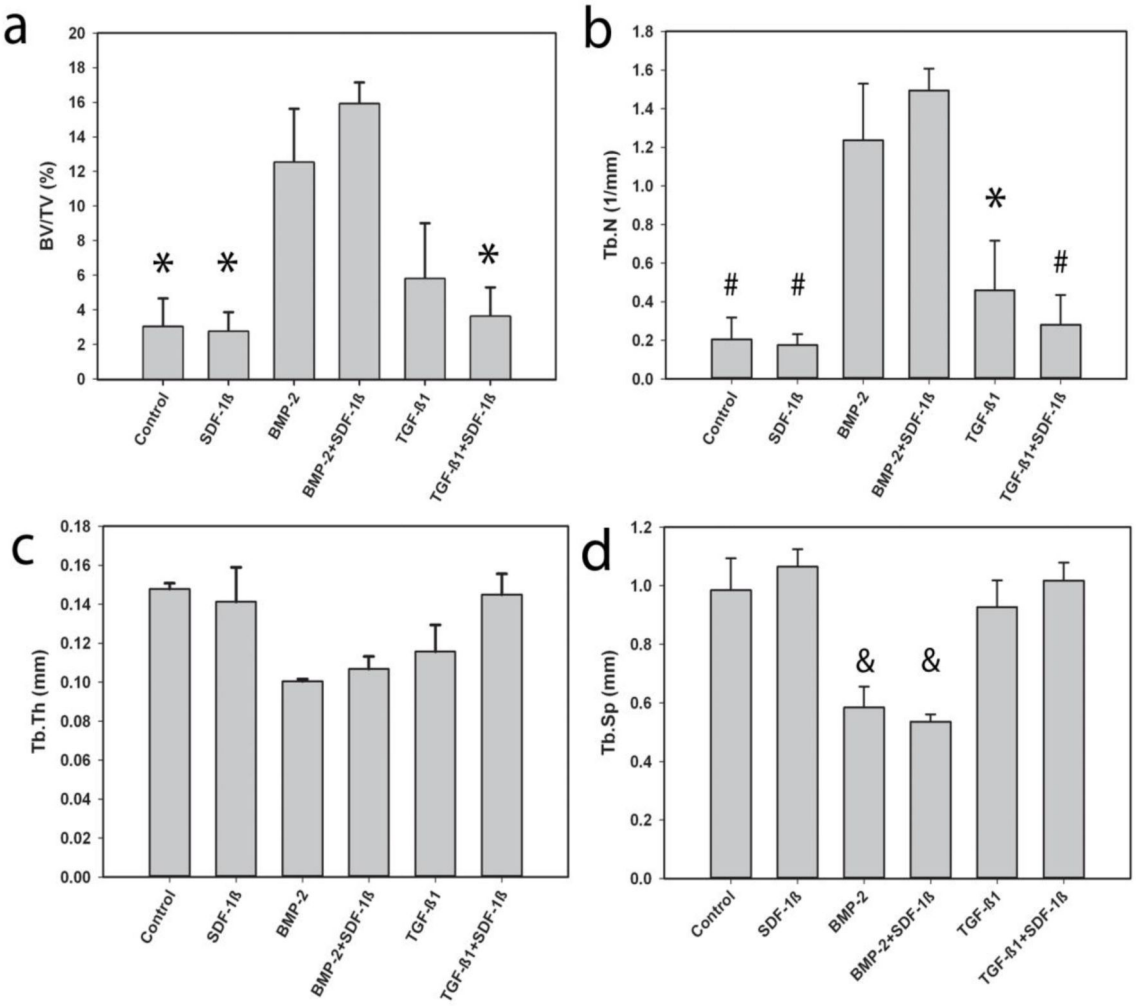

Figure 4.

a-Mean percent bone volume (BV/TV), *b*-trabecular number (Tb.N), *c*-trabecular thickness (Tb.Th), and *d*-trabecular separation (Tb.Sp) of defect by treatment, 4 weeks post-op. * indicates significant difference compared to *BMP-2+SDF-1β* group. # indicates significant difference when compared to *BMP-2* and *BMP-2+SDF-1β* respectively. & indicates a significant difference when compared to *Control*, *SDF-1β*, *TGF-β1*, and *TGF-β1+SDF-1β* respectively.

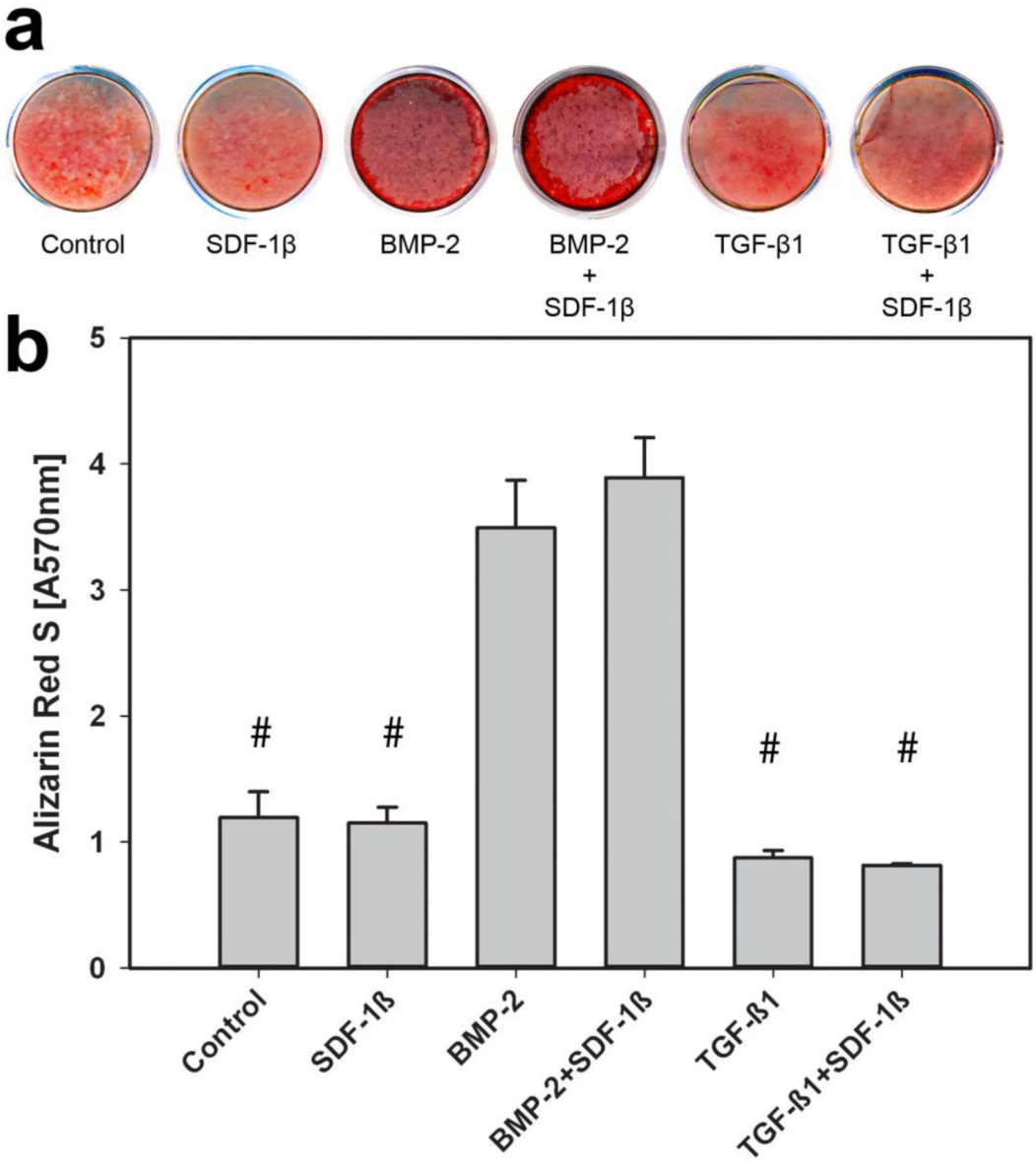

Figure 5.

Osteogenic differentiation measured by *a*-Alizarin Red S (ARS) staining and *b*- quantitative analysis, 21 days. # indicates significant difference when compared to *BMP-2* and *BMP-2+SDF-1β* respectively.

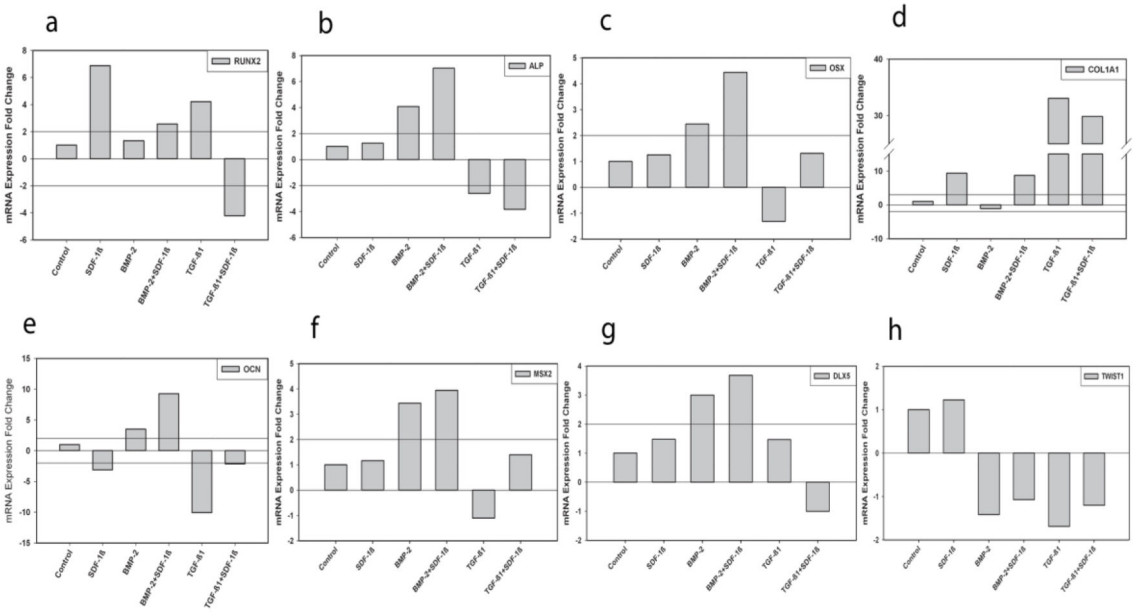

Figure 6.

qRT-PCR analysis of MC3T3-E1 cell gene expression after cytokine treatment in culture. a-Runx2, b-Alp, c-Osx, d-Col1a1, e-Ocn, f-Msx2, g-Dlx5, h-Twist1, 7 days.

Bone. Author manuscript; available in PMC 2015 October 01.

Table 1

Quantitative qRT-PCR Primer Data

Gene Symbol	Gene Name	Primer Sequence	Reverse Primer
RUNX2	Runt Related Transcription Factor 2	Mm00501584_m1	GAGCCAGGCAGGTGCTTCAGAACTG
OCN	Osteocalcin	Mm01741771_g1	CAGACAAGTCCCACACAGCAGCTTG
Col1a1	Collagen, Type I, alpha 1	Mm00801666_g1	CGATGGATTCCCGTTCGAGTACGGA
ALP	Alkaline Phosphatase	Mm00475834_m1	TGTGGCCCTCTCCAAGACATATAAC
MSX2	Msh Homeobox 2	Mm00442992_m1	GCCGCCCAGACATATGAGCCCCACC
DLX5	Distal-Less Homeobox 5	Mm00438430_m1	ACCAGCCAGCCAGCTTTCAGCTGGC
TWIST1	Twist Homolog 1	Mm00442036_m1	CAGGCCGGAGACCTAGATGTCATTG
OSX	Osterix	Mm04209856_m1	GCGTCCTCTCTGCTTGAGGAAGAAG
18S	18S ribosomal RNA	Mm03928990_g1	TACTTGGATAACTGTGGTAATTCTA